Cement & Concrete Composites 45 (2014) 201–208

Contents lists available at ScienceDirect

Cement & Concrete Composites

journal homepage: www.elsevier.com/locate/cemconcomp

An experimental study of the effect of CO_2 rich brine on artificially fractured well-cement

Mustafa Hakan Ozyurtkan [a,*], Mileva Radonjic [b]

[a] Petroleum and Natural Gas Engineering Department, Faculty of Mines, Istanbul Technical University, 34469 Maslak, Istanbul, Turkey
[b] Craft and Hawkins Petroleum Engineering Department, Louisiana State University, Patrick F. Taylor Hall, Baton Rouge, LA 70803, United States

ARTICLE INFO

Article history:
Received 15 October 2012
Received in revised form 25 September 2013
Accepted 4 October 2013
Available online 16 October 2013

Keywords:
Cement fractures
Hydraulic conductivity
Permeability
Dissolution
Microstructures
Well cement durability

ABSTRACT

The performance of structural seals overlying reservoirs targeted for CO_2 storage relies upon the integrity of well-bore cements, which will be affected by interactions with CO_2. Microfractures within the well-bore cement may lead to seepage of CO_2 to the surface and/or fresh water aquifers. Thus, understanding CO_2-rich brine induced changes to the imperfections in cement matrix is vital for safe and effective implementation of this new technology named Carbon Capture Utilization and Storage (CCUS).

This paper presents an experimental study that depicts the changes of the cement internal structure due to interaction with acidic brine through a system of artificial fractures within the cement matrix during 100 days flow through experiments. Helical computerized axial tomography and high resolution micro-computed tomography were used to visualize several sub-volumes of flow-through cores. Furthermore, a complementary high-resolution surface profilometry allowed quantification of changes of the roughness of fracture walls and their impact on the fracture aperture.

1. Introduction

CCUS projects require capturing carbon dioxide from large point sources such as fossil fuel power plants and other manufacturing processes that produce CO_2 and storing it in the subsurface for hundreds of years. Although CO_2 has been injected into geological formations by the oil and gas industry for enhanced oil recovery (EOR), the permanent storage of CO_2 is a relatively new concept. The long-term containment of injected gas is a critical component for effective CCUS, requiring that potential pathways for leakage be identified, investigated and risk assessment performed. CCUS technology may involve injection without offsetting production of fluids leading to potentially large pressure perturbations, particularly during the injection phase [1].

The resulting vertical pressure gradients favor leakage into overlying freshwater aquifers and/or the atmosphere. Existing wellbores with a history of wellbore integrity problems and/or sustained casing pressure have been identified as one of the most likely pathway for such leakage [2].

Investigations of the long-term interactions of acidic brine (resulting from equilibration of formation waters with injected CO_2) and wellbore cement are fundamental to understanding the integrity of existing wellbores and their long-term durability during CCUS operations. In the post injection stage, acidic brine with pH ~ 3–5 will interact with wellbore cements whose equilibrated pore fluids have pH ~ 13.5. This significant pH change will lead to changes in the cement matrix properties since most of the hydrated and unhydrated cement minerals are in equilibrium at pH > 7. The primary objective of this experimental study is to quantify mineralogical and microstructural changes of cements containing fractures after they have been subjected to a flow through regime of CO_2 rich brine for an extended time of 100 days and establish the impact of these changes on hydraulic conductivity of cements when compared to 30 days exposure previously reported by Yalcinkaya et al. [3].

1.1. Fractured wellbore cement

Cement has been used to provide zonal isolation (i.e., minimize the potential for flow through wellbores that intersect important structural seals as well as flow between different formations) in oil, gas and geothermal wells for decades. In addition, its mechanical strength enhances the geomechanical stability of the wellbore and its low permeability provides protection for metal casings against corrosive formation waters rich in salts and often CO_2 and/or H_2S. Oil, gas and geothermal wells are designed to last a few decades; conversely, CCUS projects will require wellbore cements to perform zonal isolation for hundreds of years. The second major difference between CCUS and traditional subsurface injection of CO_2 in EOR is the volume and injection pressure, both of which will be much higher and without any production of fluids

* Corresponding author. Tel.: +90 212 285 62 61; fax: +90 212 285 62 63.
E-mail address: ozyurtkan@itu.edu.tr (M.H. Ozyurtkan).

0958-9465/$ - see front matter © 2013 Elsevier Ltd. All rights reserved.
http://dx.doi.org/10.1016/j.cemconcomp.2013.10.007

to offset the potential pressure buildup, especially during the injection – early stages of CCUS.

The zonal isolation provided by wellbore cements aims to prevent fluid entry into wellbores except in the perforated sections within production and injection zones. However Sustained Casing Pressure (SCP), defined as the casing pressure caused by trapped gas or liquid in the annulus, is recorded in the field as a direct manifestation of inadequate cementing. This causes major technical and economic problems during plugging and abandonment (P&A). However, CCUS technology is based on injection of large volumes of fluid therefore pressure buildup is likely to occur during injection period and can potentially cause faster SCP manifestation, resulting potentially in a rapid gas release.

Wellbore cement failures can take place both during and/or after cementing operations. Inappropriate cement slurry design or inadequate mud removal prior to cementing may result in weak bonding at cement/casing and/or cement/formation interfaces. Such conditions may result in the formation of gas channels within cement column. The set cement is further subjected to unsteady loads as a result of continuous pressure and temperature cycles during production and injection operations as well as various wellbore testing procedures [4].

The cement matrix has different thermal expansion and elasticity coefficients than the casing and adjacent rock formations. Variable expansion rates of the above materials may lead to formation of a microannulus between the casing/rock and the cement as well as create fracture networks within set cement [5].

1.2. Cement – acidic brine chemistry

Calcium and silica are the two major elements of Portland cement, which consists of four main crystalline components: Tricalcium Silicate (Ca_3SiO_5–C_3S), Dicalcium Silicate (Ca_2SiO_4–C_2S), Tricalcium Aluminate ($Ca_3Al_2O_6$–C_3A) and Tetracalcium Aluminoferrite ($Ca_4Al_2Fe_2O_{10}$–C_4AF). As a result of hydration, Calcium Silicate Hydrates (C–S–H) and Portlandite ($Ca(OH)_2$) are formed. Furthermore, the hydration process forms other minerals such as Ettringite ($(CaO)_6(Al_2O_3)(SO_3)_3{\cdot}32\ H_2O$) [6].

When the cement matrix is exposed to CO_2-saturated brine, the following chemical reactions occur [7].

$$CO_2 + H_2O \rightarrow H_2CO_3 \quad (1)$$

$$H_2CO_3 + Ca(OH)_2 \rightarrow CaCO_3 + H_2O \quad (2)$$

$$H_2CO_3 + CaCO_3 \rightarrow Ca(HCO_3)_2 \quad (3)$$

$$Ca(HCO_3)_2 + Ca(OH)_2 \rightarrow 2CaCO_3 + 2H_2O \quad (4)$$

Once consumption of all the major Ca-containing minerals (mainly portlandite and traces of calcite) occurs, C–S–H will start leaching Ca^{2+}, leading to a formation of an amorphous silica rich gel-like material, which has a deleterious effect on the mechanical properties of the cement and more importantly an increase in porosity [6,8].

In this study we investigated stability of fully hydrated Portland cement in contact with low pH fluids under dynamic conditions. However, some of unhydrated cement clinker minerals can still exist and therefore need to be introduced, as they also can contribute for example as a source of Ca once portlandite is depleted. The second set of characteristic typical for cement that is of importance in cement-fluid interaction is porosity and permeability. Chemically unaltered cement has low permeability, primarily due to the nature of fully hydrated cement which is dominated by C–S–H and its nanoporosity. In addition porosity and permeability can be impacted by hydrostatic pressure applied to cement in the field as well as various admixtures commonly used in the field, such as fluids loss control material, weighting agents, and contaminations. Ca leaching of hydrated Portland cement is associated with an increased total porosity and expected increase in permeability [2].

2. Methodology

2.1. Flow through apparatus

The experimental set-up reported in detail by Yalcinkaya et al. [3] was used for the current study. It consisted of a Hassler cell, syringe pump, hydraulic pump, data acquisition system, filters and pressure gauges. The Hassler cell was oriented vertically to simulate the upward flow of CO_2 saturated brine through a vertically fractured cement system. To maintain continuous flow of brine, a dual syringe pump system, with a maximum capacity of 507 ml, was adjusted to single-pump auto-refill mode during the experimental period. A 100-day flow-through experiment was carried out [3].

2.2. Cement core

Class H cement, as specified by American Petroleum Institute (API) cement classification was used, as it is a most commonly used type of wellbore cement in the United States, to form the cylindrical, 1-in × 12-in (2.54 cm × 30.48 cm) cement core. Following the recommendations from API (API 10B – Recommended Practice for Testing Well Cements), a water to cement ratio of 0.38 was used for the cement slurry, utilizing deionized water. Trapped air was removed from the cement using a vacuum pump before pouring cement slurry into teflon molds. Cement slurry was poured into custom made teflon molds to cast two halves and de-molded after 24 h. The cement core halves were cured in water bath pH ~ 13 for 30 days at room temperature.

Upon hydration and curing the cement halves were glued using epoxy along the edges to obtain a 1-in × 12-in (2.54 cm × 30.48 cm) cylindrical shape with the channel in the middle. This design provided a parallel-plate-like channel along the length of the cement core. Though this design is a somewhat simplified representation of real fractures in well-bore cements, which are likely to have rough fracture walls, it provides a controlled initial fracture geometry, which allows for unambiguous observation and quantification of fracture-surface alterations as an evidence for dissolution/precipitation. Sample preparation methods are described and documented in Yalcinkaya's master thesis [9].

2.3. Reactive fluid

The brine (2% salt solution) used for the flow-through experiment consisted of distilled water mixed with NaCl and KCl salts at concentrations of 0.3455 M and 0.0046 M, respectively. The influent brine was equilibrated with CO_2 by bubbling CO_2 through the solution. The pH of the CO_2-equilibrated brine ranged from 4.9 to 5.2 and was continuously measured daily prior to entering flow-through experiment.

2.4. Experimental conditions

The experiment was performed at atmospheric pressure (14.7 psi, 0.1 MPa) and room temperature (21 °C, 70 F) conditions. The flow-through experiment lasted for 100 days. CO_2 saturated brine flow rate was 2 ml/min. The confining stress of 600 psi (4.14 MPa) was applied to the rubber sleeve containing the cement core in order to create linear flow only through the cement fracture preventing any radial flow of reactive fluids. At the end of 100 days, the pressure was gradually reduced and the cement core was re-

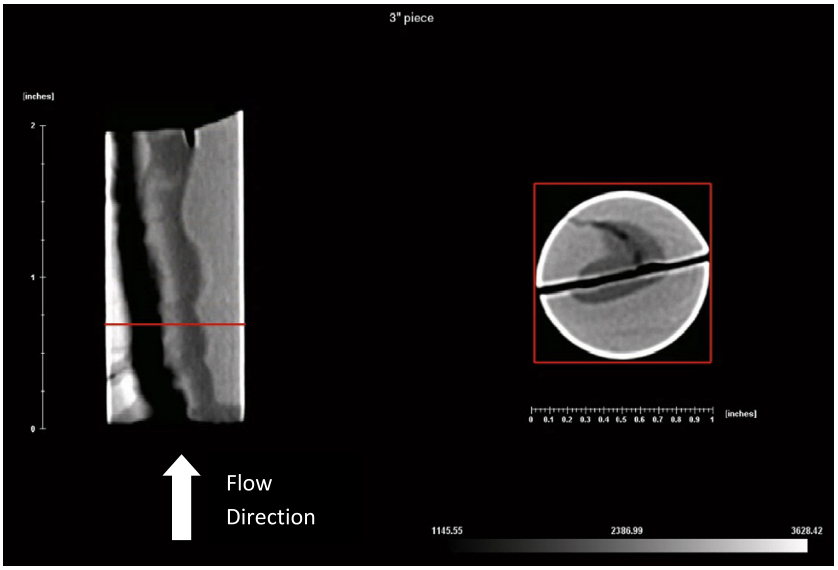

Fig. 1. Helical CT image of the inlet section of the reacted cement sample after 100 days of flow through with CO_2-rich brine. Longitudinal scan on the left shows reacted region (lower density due to Ca loss) present along the entire length of the main fracture wall. Cross-sectional view shown on the right depicts presence of secondary fracture initiated perpendicular to the main fracture wall. The secondary fracture wall has the highest level of Ca leaching at the fracture opening and it is reduced towards the fracture tip, suggesting the leaching region is depent on the width of the fracture. (The sample is 3 in. long and 1 in. wide.)

moved from the Hassler cell to perform material characterization analyses of the sample. Pressure increase at the start of the experiment and de-pressurization at the end of the experiment were performed in incremental steps over 24 h in order to avoid fracturing and rapid mineral precipitation induced by rapid pressure difference.

2.5. Material characterization

The cement core was subjected to material characterization before and after the flow-through experiment. The following materials characterization techniques were employed: Helical computerized axial tomography (Helical CT); high-resolution micro-computed tomography (microCT); x-ray diffraction (XRD); mercury intrusion porosimetry (MIP); and profilometry of the fracture surfaces. All these analyses required different sample size/morphology from cement core. In order to carry out these analyses, the cement core was cut into several sections and side micro-cores were drilled from the fracture surface into the interior part of cement for micro-CT scans.

XRD analyses were conducted in the LSU Geology Department using a Siemens Kristalloflex D5000 X-Ray diffractometer. The data acquisition was carried out within the range of well-known cement minerals 2–70 degrees at a grade of 0.02-degree increments with Cu $K\alpha_1$ radiation.

For Helical CT analysis cement core samples were scanned at 120 KV using 2006 Toshiba Acquilion 64 slice scanner. The actual output of the scanner is in video format. High-resolution X-ray tomography images were obtained at the Louisiana State University Center for Advanced Microstructures and Devices (CAMD) Tomography beam line. Mini cement cores (3 mm diameter by 5 mm length), were obtained by drilling through sections of reacted cement core (focusing on inlet and outlet sections) and scanned at 2.5 μm spatial resolution at 34 keV monochromatic X-ray energy. After scanning process, images of the slices of the mini cement core were reconstructed using a MatLab check spelling program.

Topographic mapping of fracture surfaces was carried out using an optical surface profilometer (Nanovea ST-400), at Civil and Environmental Engineering Department of The University of California, Irvine. The profilometer measures the mean elevation of 12 m-diameter spots on the surface of the sample with a reported accuracy of ±2 m. For the scans reported here we used an *x*–*y* spacing of 20 m.

3. Results and discussions

3.1. Helical computerized axial tomography (helical CT)

Helical CT was utilized to analyze two sections of the core: a 3-inch long section taken from the inlet end of the core and a 6-inch long section taken from the outlet end of the main cement core. Screen shots from the video output can be seen in Figs. 1 and 2. Lateral views can be seen on the left part of the figures and axial views, corresponding to the cross-section identified by the red[1] lines on the lateral views, on the right part of the figures. The most important observation in each of the sections is that in addition to the main fracture, which was part of the sample design, there appear to be present entire network of fractures at the outlet and one secondary fracture at the inlet section. No secondary fractures were observed at 30 days as reported in Yalcinkaya et al. [3].

The secondary fractures also appear to have highly leached cement regions (shown by darker color), which suggests that these fractures developed during flow through experiments and were not result of depressurization of the sample. Both figures show consistent alterations in the vicinity of the secondary fracture surfaces while at the main fracture walls (channel in the center of the core). These alterations are represented by the darker shades of grey in similar regions. This indicates density reduction along the secondary fractures wall surfaces due to leaching of chemical components with higher atomic mass, in this case Ca, Fe. The mechanism appears to be different from one reported after 30 days flow through experiment, where only widening of the main fracture aperture was evident, Yalcinkaya et al. [3].

[1] For interpretation of color in Figs. 1, 2 and 7, the reader is referred to the web version of this article.

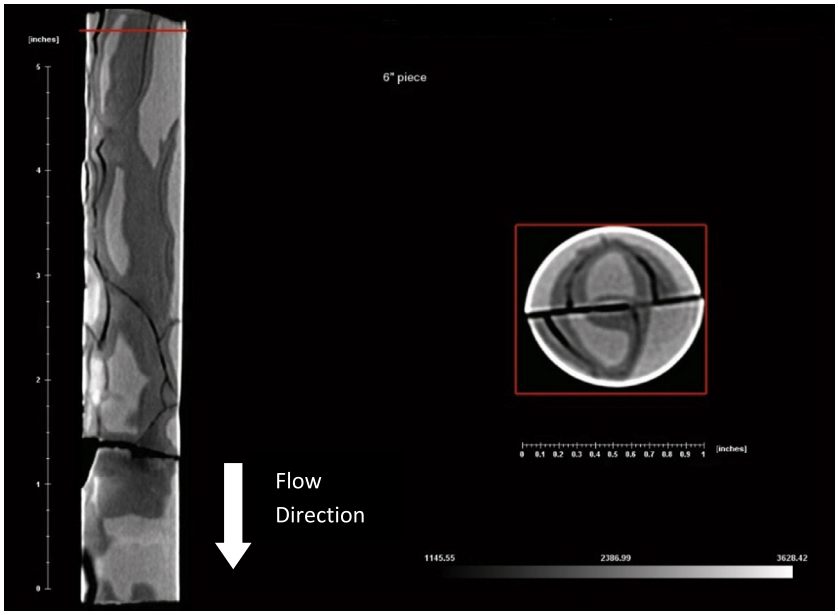

Fig. 2. Helical CT image of the outlet section of the reacted cement sample after 100 days of flow through with CO_2-rich brine. Longitudinal scan on the left shows reacted region (lower density due to Ca loss) present along the entire length of the main fracture wall. Cross-sectional view shown on the right depicts presence of secondary fracture initiated perpendicular to the main fracture wall. The secondary fracture wall has the highest level of Ca leaching at the fracture opening and it is reduced towards the fracture tip, suggesting the leaching region is dependent on the width of the fracture. (The sample is 6 in. long and 1 in. wide.)

The second notable observation is that the secondary fracturing is more frequent at the outlet than inlet section, and although inlet section is shorter there is only one secondary fracture present along 3 in. section. Finally, it is worth examining the orientation of the secondary fractures, as they are always initiated perpendicular to the main fracture. The aperture of secondary fractures is almost identical to the width of the primary fracture (channel) manufactured in the center of the core during sample assemblage.

3.2. High resolution micro-computed tomography

Given the 2.5 μm voxel size of the microCT images, it is only capable of recognizing features that are 5 μm or larger. Two sub volumes were selected for reacted samples; one in region A and one in region B for both inlet and outlet sample sections. These sections are shown in Fig. 3. Increased slice number indicates that images are taken closer to the fracture surface and lower slice numbers are further from cement-fluid interaction region and closer to the edge of cement core. As it can be observed, top two images display almost uniform density and only peripheral signs of reactivity at the edge of the core, which is most likely an artifact due to the beam curving effect. The bottom two images taken from the opposite end of the micro-core and at the fracture wall show also a uniform low density, as these regions were primarily leached of Ca, whose main source was calcium hydroxide (portlandite). The result is higher porosity (originally occupied by large hexagonal plates of portlandite) and overall lower atomic density of remaining phases, such as C–S–H. In the middle section of the core dissolution of portlandite is not uniform and the images are showing partial loss of Ca (region A). The spatial distribution of two regions is not uniform, suggesting that dissolution takes place in preferential directions, it does not have previously reported ring-like zonal appearance typical for diffusion driven reaction. Finally, comparing inlet (left column) to the outlet (right column) images, there is not a major difference in alterations, they are very similar in the type of density present as well as distribution of reacted vs unreacted regions. Therefore it seems that the difference present at the larger scale shown in previous section is not evident at the microscale acquired in MicroCT.

Fig. 4 represents the density change in the *z*-direction from fracture surface to the inner part of the cement core (cross-sectional view). The black-white color in CT images represent low-high density of the phases present respectively, where 100% black represents void space (porosity). Different degrees of grey are representing variation in chemical composition, primarily Ca/Si ratio, and bright (white) areas are depicting Fe-rich minerals as the highest density components in hydrated cement.

3.3. Image based calculated porosity

The grayscale images were transferred to binary images (solid and void) using a simple thresholding algorithm in ImageJ program. After identifying the solid and void phases, the porosity was determined by calculating the volume fraction of each phase. The porosity values were found for inlet section 0.029% and 0.018% in regions A and B, for the threshold values 75 and 45 respectively. Similar porosity reduction was observed for outlet section with porosity values of 0.039 and 0.032 in regions A and B, for the threshold values 65 and 30 respectively. Table 2 tabulates the calculated image-based porosity values obtained from high-resolution X-ray tomography scans. For image based analysis, porosity was defined as the volume fraction of void space that contains pores on the order of 5 μm or larger. As it can be seen from Table 1, in region A which is in direct contact with low pH brine, there is an evident increase of porosity, in both inlet and outlet section of cement core, when compared to unreacted region B, located further from cement-fluid contact.

3.4. Surface profilometry

Surface profilometry measurements provided a detailed map of changes in the surface topography of the fracture wall caused by dissolution/precipitation of mineral phases as a result of cement/flowing brine interaction. Fig. 5 shows surface elevation maps of

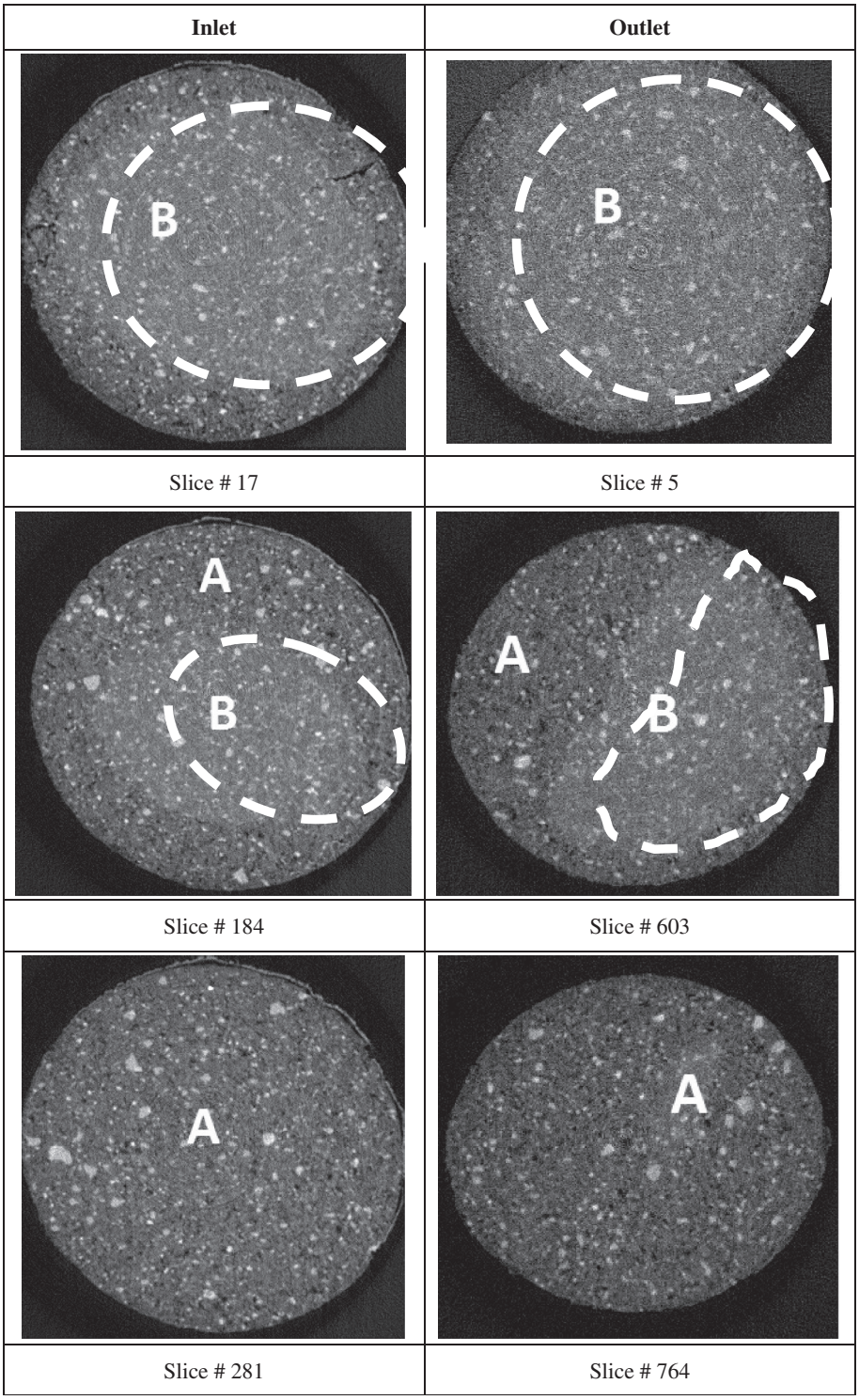

Fig. 3. Micro-CT Images (axial slices) of Reacted Cores for Inlet and Outlet Sections. (There are two distinct regions marked as A and B. Regions A have darker color indications lower atomic density. Regions B are brighter color showing unreacted regions of cement sample with minimal or no alteration due to cement-fluid interaction.)

a fracture surface before the flow-through experiment (a) and a segment of the core taken from the inflow end after the flow-through experiment (b). There are regions of significant erosion observed in the post-experiment surface, including the apparent formation of a connected region of relatively low elevation oriented along the length of the core. This low elevation region is indicative of a growth of a dissolution channel similar to those observed in simpler systems involving reactive transport through fractures [10].

Prior to the experiment, the surface roughness ranged over less than 50 m and was characterized by shallow (<20 m) grooves resulting from the polishing of the surfaces and a long wavelength trend perpendicular to the axis of the core. After the experiment, surface roughness ranged over more than 1000 m and included

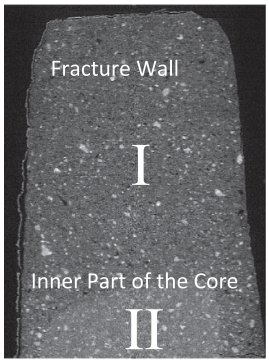

Fig. 4. Cross-sectional View of Micro-CT Image along the Length of Mini-core drilled from the inlet section. (Region I (darker color) indicates reacted regions close to the fracture wall and region II (brighter color) indicates that further from the fluid contact cement appears to be intact, no leaching of Ca.) (The width of the sample is 3 mm, and the length of the sample is 5 mm.)

Table 1
Cement sample's image based porosity values from high resolution micro-computed tomography.

Un-reacted	Reacted inlet		Reacted outlet	
Porosity	Porosity region A	Porosity region B	Porosity region A	Porosity region B
0.25%	2.9%	1.8%	3.9%	3.2%

Table 2
Total porosity values of unreacted and middle, and outlet section of the reacted samples derived from MIP measurements.

Sample identification	Total porosity (%)
Unreacted	26.33
Reacted middle section	25.77
Reacted outlet section	19.54

regions (in red in Fig. 5) where little alteration occurred and regions along what was likely the primary flow path (in blue/green in Fig. 5) where significant erosion occurred. The surface profilometry data on this section of the core did not provide any evidence of the self-healing properties of the fracture. Furthermore, surface profilometry does not depict preferential sites for secondary fracture initiations.

3.5. Mercury intrusion porosimetry

For MIP analysis two samples were taken, one from the middle section and one from the outlet section of the core. The sample taken from middle section had a measured porosity value of 26%. It is observed that during the flow through experiment, the porosity of the core reduced to 20% at outlet section of the core. Table 2 tabulates the porosity values of reacted and unreacted cement core samples.

Similar porosity values were reported by Yalcinkaya's study for a total of 30 days flow through on multiple experiments. He reported an average of 20.5% porosity for inlet and 20.426% for outlet section of the cement core. He observed a decrease in total porosity from 26% to 20% after 30 days flow through experiment [3]. MIP standard provided the pore throat size distribution ranging from 0.0018 to 70 μm. Porosity values were plotted against pore throat sizes shown in Fig. 6.

Fig. 6 presents the total pore throat size distribution (size range 0.0018–70 μm). The reduction in total porosity was observed in the range from 0.035 μm to 0.5 μm, which coincides with the highest porosity within the unreacted cement matrix.

Smallest pore throats (0.0018–0.1 μm) showed a reduction as well. However, the pore throats larger than 0.1 μm did not show a distinct alteration from unreacted to reacted cement.

When focusing on the pore throats between 0.1 μm and 0.5 μm, the porosity of the middle section was higher than the unreacted sample. However, the measured porosity values were nearly identical for the outlet section of the core and the unreacted sample (control sample).

Between 0.5 μm and 3 μm pore throat size, the porosity was higher in the unreacted sample, suggesting that these pores might have been restricted to flow or reduced as a result of experiment. However, comparing reacted regions the sample from the middle section of the cement core had higher porosity than the sample from outlet section of the cement core, which could be due to precipitation of secondary deposits from perhaps more saturated fluid once it reached the outlet. Another possible explanation is the removal of fine particles and fragments by flowing fluid and accumulation of these fines and/or amorphous matter at the outlet which has been also reported by Agbasimalo et al. [11].

MIP analysis suggested that there were no pore throats larger than 62 μm. The largest measured pore throat was 62 μm. There was an increase in the porosity of the middle range pore throat size, approximately between 10 μm and 30 μm. The porosity of the unreacted sample was higher than the porosity of middle section of the reacted core and the outlet section for the pore size range from 30 μm to 62 μm.

3.6. X-ray diffraction

Qualitative XRD analysis was conducted in order to detect mineralogical alterations as a result of brine/cement interaction using a semi-quantitative approach by comparing the peak ratios of relevant diffractograms; portlandite peaks obtained before and after the flow-through experiments, and intensity ratios of carbonate minerals were of primary interest. XRD analysis was performed on the section which was cut directly from fracture surfaces, providing altered material for analysis. Since XRD is a bulk technique averaging the amount of existing minerals in the sample (the detection level of 2 wt% of mineral present), it does not provide

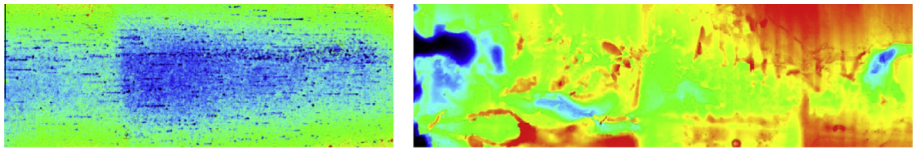

Fig. 5. Profilometry scans of 1.2-cm wide sections along the axis of the core for an unreacted fracture surface. (a) And a portion of fracture surface from the inflow end of the core after the flow-through experiment (b). The color scale (black-blue-green-yellow-red) ranges from 950 to 1000 m in (a) and from 0 to 1000 m in (b). (For interpretation of the references to colour in this figure legend, the reader is referred to the web version of this article.)

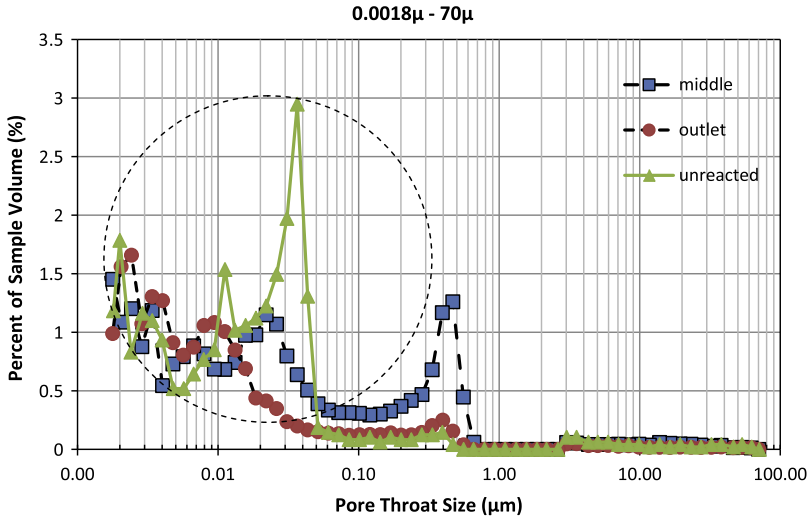

Fig. 6. Pore throat size distribution range from 0.0018 µm to 70 µm for the inlet section.

sensitivity for minute alterations. Furthermore, poorly crystalline and amorphous phases cannot be characterized, which limits detection accuracy of reaction products such as silica gel since they are non-crystalline phases. In order to have mineralogical identification localized to specific areas, we directly examined a fraction of cement taken from the fracture surface. However, calcite and portlandite are good indicators of cement reactivity for two reactions: cement carbonation and acid-attack that results in Ca-leaching.

The intensity of XRD peaks from reacted/unreacted samples is shown in Fig. 7. Diffractogram from the unreacted sample (blue, top of the figure) identifies Portlandite (P) as a main peak at ~34 degrees and calcite (CC) with a main peak at ~29 degrees. The trace from the reacted sample (bottom line, red color), has no peak for portlandite, suggesting total dissolution of portlandite. However, the amount of calcite increased to approximately 7 times its original value based on the peak ratios. Furthermore, there is a new group of peaks at 12 degrees which was not resolved due to high background, suggesting precipitation of poorly crystalline material, most likely silica-rich semi-crystalline material reported in other studies, however we did not observe a brown-red deposits typically reported in other studies on cement–acid brine reactivity [1].

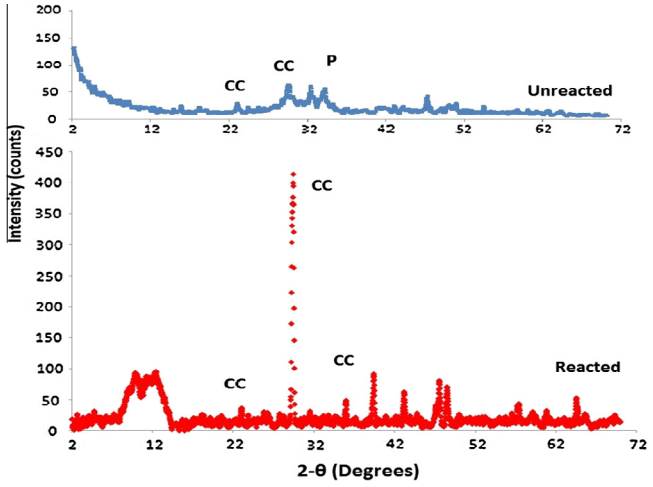

Fig. 7. XRD plot showing mineralogical alterations. (CC and P represent Calcite and Portlandite respectively).

4. Conclusions

Effects of CO_2 saturated brine on well cements under dynamic (flow through) conditions were investigated The experiment was run for 100 days as a follow up for a set of experiments carried for 30 days in order to establish the impact of time on cement-low pH brine reaction kinetics and their impact on fracture behavior [3].

The most notable difference between 30 and 100 days experimental results was development of secondary fracture network, not observed at 30 days. Secondary fractures suggest that the fracture width is correlated to the width of reacted cement adjacent to the fracture wall. At the tip of the fracture (narrower fracture aperture) cement was less affected by Ca leaching.

These density alterations along the fracture surfaces were identified by Helical CT scans. Images show alterations in the vicinity of the fracture wall-surfaces. The development of a region with characteristic darker shades of grey characterizes these alterations. Darker shades point out a reduction in density along the fracture surfaces due to dissolution of chemical components having higher atomic mass. It appears that the altered zone has increased in thickness when compared to 30 days experiments [3].

Furthermore, it was observed that overall these secondary set of fractures developed perpendicular to the original channel-fracture. This network of fractures provided an increase in hydraulic conductivity as well as enhancing total cement dissolution rates. Unlike the single fracture experiment where the total volume of cement impacted by dissolution was limited to the near fracture region, secondary fracture network allows larger volume of cement to be leached as it provides ingress of reactive fluid further into cement matrix. This can potentially have an impact on rapid deterioration of segments of wellbore cement, as the cement sheath is only 2–4 cm thick in most wellbores.

This fracture/fluid effect was also observed by MicroCT along the length of the micro-core drilled from fracture surface towards inner parts of the cement core. It has been observed that regions in direct contact with acidic brine had higher porosity compared to regions which are not in the direct contact with reactive fluid. The contact area was increased by secondary fracture network.

Similar behavior was reported by Yalcinkaya's study for 30 days flow through experiments; although the degree of alteration and the overall porosity change was lower. The porosity of the reacted and unreacted portions was observed as 1.39% and 0.45% respectively at 30 days, compared to porosity values for reacted portions

close to 3% after 100 days. However no secondary fracturing was observed at 30 days [3].

The data obtained in this study clearly indicates acidic brine negative effect on porosity of cement under dynamic conditions can greatly be impacted by time, and this is of great importance to the CCS technology which requires long term stability of cement. The next step would be to observe such changes over 6 and 12 months and based on 4 distinct data points a predictive modeling can be designed and validated.

Profilometry analysis identified regions with lower topography compared to unreacted surfaces. The presence of such regions indicates a growth of a dissolution channel parallel to flow also observed in experiments with reactive transport through fractures. At this stage it is not clear if this preferential dissolution is caused by chemical parameters or is it influenced by fluid flow regime – physical in nature, although since it is parallel to the fluid flow, it could be result of the fluid flow regime [12]. This can be determined by applying different flow rates, and observe if flow rate impacts the nature of preferential dissolution. Similar effects were also observed in 30 days experiments, although they were observed primarily using electron microscopy.

A reduction of porosity is observed in MIP data, possibly caused by secondary deposits inside the pores and/or the plugging of pore throats. To differentiate between the two a spatial imaging would be required at nanoscale, such as transmission electron microscopy (TEM). However, the overall reduction of density observed in the microCT images suggests that secondary deposits can also be attributed to Si-gel type of materials, since Ca-rich minerals should result in a higher density (brighter images). However, bulk analysis reported by XRD does show an increase in calcite and reduction of portlandite, which can be attributed to carbonation.

First of all, leaching of Ca, which takes place when cement is exposed to a pH < 13, causes porosity to increase, as observed in inlet sections of cement core flow through experiments in this study and as reported by Yalcinkaya 2010. Contrary to this, the increase of the amount of calcite and total displacement of portlandite were the major observation in XRD analysis. Once the carbonation is fully complete, the pH of the pore fluid within the hydrated cement paste reduces from ~13 to 8 with $CaCO_3$ occupying more volume than portlandite, causing a total porosity decrease. These processes may cause the permeability of the cement to decrease due to obstruction of macropores caused by carbonation [8,12–14].

MIP is a commonly used method to characterize the distribution of pore size distribution in porous materials. It is a straightforward and fast indirect method, but it has its limitations when applied to materials with irregular pore geometry. The number of pores is counted with the assumption that all pores have similar spherical shapes [15]. In spite of these limitations MIP is a valuable technique for comparing pore throats size distribution before and after acid attack on cement, especially for the pore size range that can contribute to reaction mechanisms as it is evident from the date reported that not all pores are affected by flow through experimental conditions.

Flow of acidic brine through cement core resulted in reduction of total porosity. It has been reported by numerous researchers that the reduction in porosity may be caused by two possible mechanisms: mineral precipitation inside the pores and the plugging of pore throats connecting the large pores, therefore preventing access to these larger pore volumes [6].

Acknowledgments

We would like to thank Mr. Tevfik Yalcinkaya for helping in sample preparation and experimental setup. We would like to thank to Petroleum and Natural Gas Engineering Department at ITU for their support, to Craft & Hawkins Department of Petroleum Engineering at LSU for funding this project and also to Dr. Russell Detwiller from Department of Civil and Environmental Engineering at UC Irvine for performing profilometry analyses. Tomography beamline at CAMD acknowledges the support of the monochromator and the State of Louisiana through CAMD operational budget. Also, we are thankful to Dr. Kyungmin Ham for her help performing microCT analyses at CAMD.

References

[1] Duguid A, Radonjic M, Sherer GW. Degradation of well cements exposed to carbonated brine. In: Proceedings of the 4th annual conference on carbon capture and sequestration. Washington (DC); 2005.
[2] Bachu S, Bennion BD. Experimental assessment of brine and/or CO_2 leakage through well cements at reservoir conditions. Int J Greenh Gas Control 2009;3(4):494–501.
[3] Yalcinkaya T, Radonjic M, Hughes RG, Willson CS, Ham K. The effect of CO_2-saturated brine on the conductivity of wellbore-cement fractures. In: Proceedings of the SPE international conference on CO_2 capture, storage, and utilization. New Orleans; 2010.
[4] Nelson BE, Guillot D. Well cementing. Houston: Schlumberger; 2006.
[5] Ravi K, Bosma M, Gastebled O. Improve the economics of oil and gas wells by reducing the risk of cement failure. In: Proceedings of the IADC/SPE drilling conference. Dallas; 2002.
[6] Taylor HFW. Cement chemistry. London: Academic Press; 1997.
[7] Hewlett PC. Lea's chemistry of cement and concrete. London: Elsevier; 1998.
[8] Glasser FP, Marchand J, Samson E. Durability of concrete – degradation phenomena involving detrimental chemical reactions. Cem Concr Res 2008;38(2):226–46.
[9] Yalcinkaya T. Experimental study on single cement fracture exposed to CO_2 saturated brine under dynamic conditions. Master thesis. Louisiana: Louisiana State University; 2010.
[10] Detwiler RL, Glass RJ, Bourcier WB. Experimental observations of fracture dissolution: The role of Peclet number on evolving aperture variability. Geophys Res Lett 2003;30(12):1648.
[11] Agbasimalo N, Radonjic M. Experimental study of portland cement/sandstone interface in relation to wellbore stability for carbon capture and storage. In: Proceedings of the 31st international conference on ocean, offshore and arctic engineering. Rio de Janeiro; 2012.
[12] Van Gerven T, Cornelis G, Vandoren E, Vandecasteele C. Effects of carbonation and leaching on porosity in cement-bound waste. Waste Manage 2007;27(7):977–85.
[13] Balonis M, Glasser FP. The density of cement phases. Cem Concr Res 2009;39(9):733–9.
[14] García-González CA, Hidalgo A, Fraile J, López-Periago AM, Andrade C, Domingo C. Porosity and water permeability study of supercritically carbonated cement pastes involving mineral additions. Ind Eng Chem Res 2007;46(8):2488–96.
[15] Abell AB, Willis KL, Lange DA. Mercury intrusion porosimetry and image analysis of cement based materials. J Colloid Interface Sci 1999;211:39–44.